Am J Physiol Regul Integr Comp Physiol 294: R1092–R1102, 2008.
First published December 19, 2007; doi:10.1152/ajpregu.00718.2007.

Molecular detection and immunological localization of gill Na^+/H^+ exchanger in the dogfish (*Squalus acanthias*)

James B. Claiborne,[1,2] Keith P. Choe,[2,3] Alison I. Morrison-Shetlar,[4] Jill C. Weakley,[1] Justin Havird,[3] Abe Freiji,[1] David H. Evans,[2,3] and Susan L. Edwards[1,2,5]

[1]*Department of Biology, Georgia Southern University, Statesboro, Georgia;* [2]*Mount Desert Island Biological Laboratory, Salsbury Cove, Maine;* [3]*Department of Zoology, University of Florida, Gainesville;* [4]*Department of Biology, University of Central Florida, Orlando, Florida; and* [5]*Department of Biology, Appalachian State University, Boone, North Carolina*

Submitted 4 October 2007; accepted in final form 12 December 2007

Claiborne JB, Choe KP, Morrison-Shetlar AI, Weakley JC, Havird J, Freiji A, Evans DH, Edwards SL. Molecular detection and immunological localization of gill Na^+/H^+ exchanger in the dogfish (*Squalus acanthias*). *Am J Physiol Regul Integr Comp Physiol* 294: R1092–R1102, 2008. First published December 19, 2007; doi:10.1152/ajpregu.00718.2007.—The dogfish (*Squalus acanthias*) can make rapid adjustments to gill acid-base transfers to compensate for internal acidosis/alkalosis. Branchial Na^+/H^+ exchange (NHE) has been postulated as one mechanism driving the excretion of H^+ following acidosis. We have cloned gill cDNA that includes an open reading frame coding for a 770-residue protein most homologous (~71%) to mammalian NHE2. RT-PCR revealed NHE2 transcripts predominantly in gill, stomach, rectal gland, intestine, and kidney. In situ hybridization with an antisense probe against NHE2 in gill sections revealed a strong mRNA signal from a subset of interlamellar and lamellae cells. We developed dogfish-specific polyclonal antibodies against NHE2 that detected a ~70-kDa protein in Western blots and immunologically recognized branchial cells having two patterns of protein expression. Cytoplasmic and apical NHE2 immunoreactivity were observed in cells coexpressing basolateral Na^+-K^+-ATPase. Other large ovoid cells more generally staining for NHE2 also were strongly positive for basolateral H^+-ATPase. Gill mRNA levels for NHE2 and H^+-ATPase did not change following systemic acidosis (as measured by quantitative PCR 2 h after a 1- or 2-meq/kg acid infusion). These data indicate that posttranslational adjustments of NHE2 and other transport systems (e.g., NHE3) following acidosis may be of importance in the short-term pH adjustment and net branchial H^+ efflux observed in vivo. NHE2 may play multiple roles in the gills, involved with H^+ efflux from acid-secreting cells, basolateral H^+ reabsorption for pH_i regulation, and in parallel with H^+-ATPase for the generation of HCO_3^- in base-secreting cells.

acid-base regulation; branchial; elasmobranch; sodium/hydrogen antiporter

ACID-BASE REGULATION in fishes is primarily accomplished by epithelial transfer of relevant ions (H^+ and HCO_3^-) across the gills (17, 32). Because of their low plasma P_{CO_2} and HCO_3^- concentration (on the order of 2–4 torr and 4 meq/l, respectively) and relatively low plasma buffer capacity, typical mammalian ventilatory adjustments to modify plasma P_{CO_2} are not available to these aquatic animals. Internal pH must be adjusted by the differential excretion of H^+ and HCO_3^- to the ambient water (see reviews in Refs. 19, 33, and 44). Because of their hyperionic environment, marine fishes are also faced with a diffusive ion influx of salt (predominantly NaCl) that must be balanced by active excretion to the water. The maintenance of internal acid-base equilibrium may also impact this ionic balance when the transfers of H^+ and HCO_3^- are linked to Na^+ and Cl^- movements (17). Unlike mammals, the kidneys play little role in these transfers in most species measured, but the ion transport mechanisms postulated for the gill epithelium are analogous to those hypothesized for the mammalian renal tubule. In saltwater-adapted teleost fish, apical Na^+/H^+ exchange (NHE) and Cl^-/HCO_3^- exchange are thought to drive acid-base transfers across the gills, whereas salt excretion is accomplished via the Na^+-K^+-$2Cl^-$ cotransporter and apical cystic fibrosis transmembrane conductance regulator Cl^- channels, with Na^+ moving to the water through paracellular junctions (reviewed in Ref. 26). The driving force for the system is the low intracellular Na^+ concentration maintained by basolateral Na^+-K^+-ATPase. In this model, excretion of acid-base relevant ions will add to the NaCl load that the animal must ultimately excrete (23).

Marine elasmobranches present an intriguing model for understanding the mechanisms of fish epithelial acid-base transfers, because salt excretion is predominantly accomplished by an extrarenal salt gland (the rectal gland), whereas acid-base exchanges occur nearly completely across the branchial tissues (41, 54). Several species (20, 34) have been shown to adjust rapidly to either metabolic or respiratory acidosis by utilizing gill-to-water H^+ transfers. For example, we found that the spiny dogfish shark (*Squalus acanthias*) could recover nearly completely from hypercapnia over 24 h by net H^+ excretion to the water to raise plasma HCO_3^- and compensate the serosal pH decrease (20). Restoration of water P_{CO_2} to normal levels resulted in a rapid loss of the accumulated plasma HCO_3^- to the water and a return of plasma pH to prehypercapnic controls. The majority of acid-base transfers are extrarenal (54). It has only been over the past few years that molecular and biochemical approaches have begun to reveal the gill transport mechanisms that may be involved.

The gill of the little skate (*Raja erinacea*) has significant H^+-ATPase activity that can be inhibited by *N*-ethylmaleimide (37). Wilson et al. (65) used polyclonal antibodies against bovine vacuolar H^+-ATPase to identify cells expressing this enzyme in the gill of the dogfish. The immunolocalized cells were in the interlamellar regions of the gill filaments and exhibited an ultrastructure similar to mitochondrial-rich cells when viewed at the electron microscopic level. More recent

Address for reprint requests and other correspondence: J. Claiborne, Dept. of Biology, Georgia Southern Univ., Statesboro, GA 30460 (e-mail: jb@georgiasouthern.edu).

The costs of publication of this article were defrayed in part by the payment of page charges. The article must therefore be hereby marked "*advertisement*" in accordance with 18 U.S.C. Section 1734 solely to indicate this fact.

0363-6119/08 $8.00 Copyright © 2008 the American Physiological Society

Downloaded from ajpregu.physiology.org on March 4, 2008

studies support the model of two distinct mitochondrial-rich cell types, one expressing Na^+-K^+-ATPase and involved with H^+ excretion and the other using basolateral H^+-ATPase to drive apical HCO_3^- excretion (10, 47, 56). Piermarini et al. (48) showed that H^+-ATPase cells also expressed apical pendrin-like Cl^-/HCO_3^- exchangers and suggested that these cells could contribute to base excretion in a fashion similar to the B-type intercalated cells (51). Tresguerres and coworkers (56) also demonstrated immunolocalization of H^+-ATPase in gill cells of the pacific dogfish (*S. acanthias*) that were predominantly distinct from those expressing Na^+-K^+-ATPase, and H^+-ATPase expression increased in animals exposed to metabolic alkalosis. These authors have recently proposed that translocation of existing H^+-ATPase to the basolateral membrane of the gill-transporting cells may drive a compensatory proton reabsorption following postfeeding alkalosis (57, 58).

The Na^+/H^+ antiporter is thought to catalyze the electroneutral transmembrane exchange of sodium and hydrogen to assist in maintaining homeostasis of cell volume, intracellular/extracellular pH, and epithelial ion translocation (70). To date, 11 NHE isoforms (NHE1-11) have been identified in mammals, and orthologs exist across the animal kingdom as well as in plants, fungi, and bacteria (5). NHE1-5 have been localized to the plasma membrane, with NHE2 and NHE3 normally apically expressed and involved in luminal Na^+ reabsorption and H^+ excretion. In mammals, NHE2 is primarily found in skeletal muscle, kidney, and the gastrointestinal tract, whereas NHE3 is mainly in the renal tubule, intestine, and stomach (39, 70). NHE3 is the predominant apical exchanger in the renal proximal tubule and is upregulated during metabolic acidosis (43, 68), whereas NHE2 may be the predominant isoform in the distal convoluted tubule (63) and apical membranes of colonic crypts (30). Phylogenetic analysis of the NHE family indicates that NHE1, NHE2, and NHE4 are closely related (all belonging to the resident plasma membrane NHE clade; see Ref. 5). Generally, NHE2 is not as well studied as NHE3 and appears to play roles for both apical Na^+ reabsorption as above and pH_i regulation on the basolateral membrane (50). Interestingly, NHE2 (as well as NHE1 and -4) is thought to have first appeared in early vertebrates (5) and a partial sequence most homologous to NHE2/4 has been cloned in the stingray (Genebank no. AY626249; see Ref. 12). Thus the dogfish may present an important opportunity to characterize the function of the NHE2 isoform in its earliest form.

As implicated in teleosts (6, 18, 35), the Na^+/H^+ antiporter also may be involved in elasmobranch acid excretion across the gills. H^+ efflux in *R. erinacea* is sensitive to reductions in external Na^+ concentration, and external amiloride also inhibits skate acid excretion (22, 24). Choe et al. (12) were the first to use species-specific antibodies against NHE3 in an elasmobranch (the stingray, *Dasyatis sabina*). They demonstrated that apical NHE3 is likely involved with sodium uptake in freshwater adapted fish and is colocalized with cells also expressing high levels of Na^+-K^+-ATPase. This same pattern of distribution of NHE3 and Na^+-K^+-ATPase has also been recently described in the gills of *S. acanthias* (10). Earlier work using heterologous antibodies (against mammalian NHE2 sequence) demonstrated NHE2 immunoreactivity colocalized with Na^+-K^+-ATPase in the gills of several elasmobranch species (21) and increased protein detection following acid infusion (56). A detailed molecular and immunological characterization of elasmobranch-specific NHE2 has not been done to date.

Thus it appears that NHE may play a role in gill ion transfers in elasmobranches. We report here the cloning of a full-length NHE2-like sequence from the dogfish (*S. acanthias*) and the localization of branchial cells expressing this transcript with probes for both the NHE2 mRNA and shark-specific antibodies developed against the sequence. We have used immunohistochemical techniques with both light and confocal laser microscopy to colocalize NHE2 expression in combination with both the Na^+-K^+-ATPase and H^+-ATPase. The NHE2 immunoreactivity was detected in both Na^+-K^+-ATPase and H^+-ATPase immunoreactive cells in the gill epithelium. NHE2 mRNA levels were similar in both controls and animals exposed to an acute acidosis.

METHODS AND MATERIALS

Animals. Spiny dogfish (*S. acanthias*) were caught off the coast of Maine by commercial fishermen and transferred to large (20,000 l) aquaria at the Mount Desert Island Biological Laboratory (MDIBL). Seawater (15–19°C) was pumped continuously from Frenchman Bay into the aquaria via the MDIBL running seawater system. The tank was exposed to ambient light cycles during the summer months. Male dogfish (1–3 kg) were maintained unfed in the large holding aquarium for 3–7 days and then quickly removed and killed by brain and spinal pithing. Tissues were immediately removed for processing as described below. In some experiments, animals were anesthetized in MS-222 in seawater (150 mg/l) and the gills were perfused with cold (~4°C) elasmobranch Ringer (28) to remove blood from the gills. Once most of the blood was cleared, the animals were pithed, and gill arches (normally the second and third) were removed and prepared for Western analysis or immunohistochemistry.

Molecular cloning and sequence analysis. Total RNA was prepared from tissues homogenized in Tri-Reagent (Molecular Research Center), cDNA was generated in a reverse transcription reaction (SuperScript II; Invitrogen), and a PCR product was obtained using a degenerate primer pair specific for conserved (putative membrane spanning) areas of mammalian NHEs (3F: 5′-AAY GAY GSN GTN CAN GTN GT-3′ and 4R: 5′-GGN CKN ATN GTN ATN CCY TG-3′ where Y=C/T, S=G/C, K=G/T) first designed by Towle et al. (55). The PCR cycle parameters were as follows: 5 min at 91°C, 40 cycles consisting of 1 min at 95°C, 1 min at 45°C, and 1.5 min at 72°C, and final 7-min extension at 72°C. A BLAST search indicated that the resulting sequence of the ~700-bp RT-PCR fragment was most homologous to mammalian NHE2, and a series of specific nested primers were then designed for use in 3′ and 5′ rapid amplification of cDNA ends (RACE; Invitrogen). RACE products were subcloned (Promega and Invitrogen) and sequenced at the MDIBL Marine DNA Sequencing Center. An open reading frame (ORF) was constructed from overlapping fragments (MacVector).

The 3′ end of the gill NHE2 sequence was used to design specific primers (NHE2-F3: 5′-GGT GTC ATC ATC TGC TTC CCT G-3′ and NHE2-B3: 5′-TGG ATT CCT ATT GTT CTC CCT TCG-3′) for PCR screening of various shark tissues in paired PCR reactions with shark-specific actin primers (actin-F3: 5′-TGA AGC CCA GAA GCA AGAGAG G-3′ and actin-B4: 5′-GCT CGT TGT AGA AGG TGT GAT GCC-3′) that we developed to serve as positive controls from partial dogfish actin cDNA sequence (NCBI no. ES452223). PCR cycling parameters were as follows: initial denaturation temperature of 95°C for 1 min followed by 35 cycles of 95°C for 1 min, 57.5°C for 1 min, 72°C for 1 min, and a final extension for 10 min at 72°C. As expected, the cDNA obtained from the dogfish gill yielded a band of ~468 bp with the NHE primers (corresponding with residues 1746-2213 of the ORF) and 115 bp for actin. PCR products were confirmed by direct sequencing.

Downloaded from ajpregu.physiology.org on March 4, 2008

The predicted amino acid sequence from the dogfish NHE ORF was aligned with mammalian and fish NHE sequences downloaded from NCBI. Phylogenetic "best trees" were constructed (MacVector) using the neighbor-joining method with Poisson correction and calculation of absolute differences and bootstrap confidence estimates (10,000 replications). Predicted transmembrane regions from the dogfish sequence were calculated with hydrophilicity analysis and the Argos helix transmembrane flexibility model (1).

RNA probes. A shark NHE2 542-bp cDNA fragment (position 1746–2287 of the dogfish ORF) was inserted into RNA expression vector pGem TEasy (Promega). RNA expression vector was then linearized by restriction enzymes *Sac*II and *Spe*I to allow in vitro run off synthesis of both sense and antisense RNA probes. Generation of both sense and antisense digoxigenin (DIG)-labeled RNA probes was accomplished using in vitro transcription as per the DIG-RNA labeling kit (Roche Applied Science).

In situ hybridization. Tissue sections were postfixed in 4% paraformaldehyde in diethyl pyrocarbonate (DEPC)-treated PBS for 10 min and then rinsed for 2 × 15 min in PBS with 0.1% DEPC followed by 15 min in 5× NaCl-sodium citrate (SSC). Sections were then placed into prehyb [4× SSC containing 50% (vol/vol) deionized formamide] for 2 h. Prehyb solution was drained from the slides, and slides were then placed in hybidization buffer (40% deionized formamide, 10% dextran sulfate, 1× Denhardt's solution, 4× SSC, 10 mM dithiothreitol, 1 mg/ml yeast tRNA, and 1 mg/ml salmon sperm DNA) containing 10 ng/ml labeled sense or antisense mRNA (generated from the PCR product as above) and incubated in a humid chamber overnight at 42°C. Tissue sections were immersed in 2× SSC in a shaking water bath at 37°C for 2 × 15 min and then 1× SSC 2 × 15 min. Sections were then equilibrated in washing buffer (Boehringer Mannheim) for 5 min at room temperature followed by an overnight incubation in anti-DIG antibody diluted 1:5,000 in blocking reagent at room temperature. Sections were washed 2 × 15 min in washing buffer (BM) and then equilibrated for 5 min in detection buffer. Labeled NHE2 mRNA was visualized with nitro blue tetrazolium chloride (NBT)/5-bromo-4-chloro-3-indolyl phosphate, toluidine salt (BCIP) for 2 h, and the reaction was stopped with Tris EDTA (TE) buffer, pH 8, following counterstaining with 0.1% nuclear fast red. Sections were mounted using an aqueous mounting medium.

Antibodies. Mouse monoclonal antibody α_5 was made against the α-subunit of avian Na^+-K^+-ATPase and binds to all isoforms. It was developed by Dr. Douglas Fambrough and was obtained from the Developmental Studies Hybridoma Bank under the auspices of the National Institute of Child Health and Human Development of the University of Iowa, Department of Biological Sciences (Iowa City, IA). This antibody recognizes fish Na^+-K^+-ATPase and is now used widely for studies on fish branchial cells (6, 11, 13, 21, 46, 47, 66).

Rabbit polyclonal antibody for vacuolar H^+-ATPase (HAB) was developed by Filippova et al. (27) and was a gift from Sarjeet Gill at the University of California Riverside. It was made against a 279-amino acid peptide that matches residues 79-357 of *Culex quinquefasciatus* B subunit. This antibody has been used to localize V-H^+-ATPase in Atlantic stingrays (14, 47) and the marine long-horned sculpin (*Myoxocephalus octodecimspinosus*; see Ref. 6).

Squalus specific rabbit polyclonal antibodies against amino acids 636–654 of the dogfish NHE2 sequence (NENQVKEILIRRHESLRES; see Fig. 2) were created (BioSource International) from two different rabbits: 540 and 541 and also used in affinity-purified form (540-AP and 541-AP).

Western blotting. Gill filaments from three dogfish were removed, weighed, and placed in ice-cold homogenization buffer (250 mM sucrose, 1 mM EDTA, 30 mM Tris, 100 μg/ml phenylmethylsulfonyl fluoride, and 5 mg/ml protease inhibitor cocktail). The solution was centrifuged with the resulting pellet suspended in a 50:50 solution of homogenizing buffer and modified Laemmli sample buffer. Total protein (70 μg) was resolved on a 7.5% polyacrylamide gel and transferred to polyvinylidene difluoride membranes. The membrane was blocked with 5% Blotto (pH 7.4) for 1 h at room temperature (RT) and then incubated with either plasma from rabbits immunized against NHE2 (primary antibody 540; 1:5,000; diluted in 5% Blotto) or the affinity-purified version (540-AP; 1:7,500) overnight and washed with primary antibody (TBST: TBS with 0.1% Tween 20, pH 7.4). A secondary 1-h incubation in AP-conjugated goat anti-rabbit IgG (diluted 1:3,000 in 5% Blotto) was followed by a secondary antibody wash with 1× TBST with three changes. Bound IgG was detected using an enhanced chemiluminescence system (Bio-Rad 170-5018).

Immunohistochemistry and florescence microscopy. Gill filaments from three dogfish were removed from the arches and placed in fixative (3% paraformaldehyde, 0.05% glutaraldehyde, and 0.05% picric acid in 10 mmol/l PBS, pH 7.3) for 24 h at 4°C. Immunohistochemistry was done on frozen sections as described previously (11), with minor modifications. After 24 h of fixation, filaments were rinsed in at least three changes of PBS at 4°C, cryoprotected in at least two changes of 20% sucrose and 5% polyethylene glycol, and frozen in optimum cutting temperature embedding medium (TissueTek, Sakura, CA) by immersion in 2-metylbutane chilled with liquid N_2. Cryosections (8–10 μm) were cut longitudinally through the trailing half of filaments with a Reichert-Jung cryostat and dried on positively charged slides (Fisher Scientific). Slides were then stored at −80°C for 1–6 days. For immunostaining, slides were thawed at RT, and a hydrophobic barrier was created around each section with a PAP-pen (Electron Microscopy Suppliers). Endogenous peroxidase activity was inhibited by incubating with 0.3% H_2O_2 in block (1.5% normal goat serum, 0.09% NaN_3, and 0.1% Tween 20 in PBS at pH 7.3) for 30 min at RT. Nonspecific binding sites on the tissues were blocked by incubating with block for 30 min.

Sections were then incubated with primary antibodies and diluted in block [α_5 (1:500–1,000)], HAB (1:7,500–1:10,000), or NHE2 (540, 541: 1:5,000; 541-AP: 1:750–1:1,000) overnight at 4°C in a humidified chamber. Alternatively, negative control sections were incubated with block lacking antibodies. Unbound primary antibodies were removed with a 10-min rinse in PBS. Sections were then incubated with Vector Laboratories' biotinylated goat anti-mouse (α_5) or goat anti-rabbit (HAB and NHE2) secondary antibodies diluted in block for 30 min at RT. After being rinsed for 10 min in PBS, sections were incubated with Biogenex's ready-to-use horseradish peroxidase avidin-biotin solution for 30 min at RT. After a final wash in PBS for 10 min, antibody binding was visualized by incubating with Vector Laboratories' 3,3′-diaminobenzidine tetrahydrocholride (DAB) or vasoactive intestinal peptide substrates for 2–5 min at RT. Sections were then rinsed with running tap water for 5 min, dehydrated in an ethanol-Citrosolv series, and mounted permanently with a cover slip using permount (Fisher Scientific).

Gill sections were prepared for immunofluorescent detection using a modified protocol. Sections were deparaffinized, rinsed in PBS, and then incubated overnight in a mixture containing dilutions of each primary antibody as described earlier at 4°C. Sections were washed in PBS and then incubated in a secondary TRITC antibody mixture or Alexa Fluor 488-goat anti-mouse IgG (1:3,000) and FITC or Alexa Fluor 568 goat anti-rabbit IgG (1:3,000) (Sigma-Aldrich, St. Louis, MO, and Molecular Probes, Carlsbad, CA). Sections were mounted using buffered glycerol, and sections were visualized using an Olympus Fluoview 300 laser scanning point source confocal microscope.

Excess antigen staining controls for antibody 541-AP were done as above, except for the primary antibody incubations. 541-AP was diluted to 1.25 μg/ml (1:750) in block that also contained 250 μg/ml of NHE2 antigen. This antibody and peptide mixture was allowed to incubate at RT for 30 min before addition to gill sections.

Acidosis experiments and real-time PCR. Following MS-222 anesthesia, dogfish were cannulated via the dorsal aorta and allowed to recover in a darkened Plexiglas aquarium fed with running seawater according to the methods of Claiborne and Evans (20). After an

Downloaded from ajpregu.physiology.org on March 4, 2008

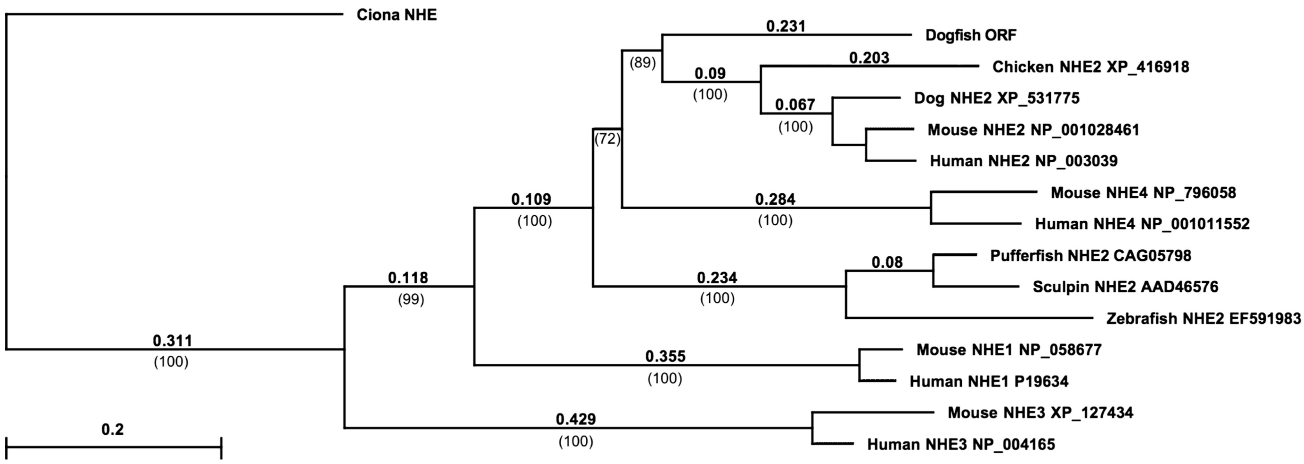

Fig. 1. Phylogenetic "best tree" using neighbor joining method with Poisson correction (bootstrap with 10,000 replications) of selected Na^+/H^+ exchanger (NHE) 1–4 sequences and the dogfish open reading frame (ORF) rooted to *Ciona intestinalis* NHE sequence (Ensemble gene prediction ENSCING00000009555). NCBI accession nos. are listed adjacent to each sequence. The length of connecting lines is proportional to the relationship, and the scale above each branch line indicates absolute differences between the amino acid sequences (1.0 = sequence is completely different, 0.0 = sequence is identical). Bootstrap confidence estimates are shown in parentheses below each node.

overnight recovery, blood samples were drawn for measurement of control pH, and then fish were infused via the dorsal aorta cannula with either Ringer (n = 5) or 1 mmol/kg HCl in Ringer (n = 5) over 1 h using a protocol similar to that of Swenson et al. (53). Blood was then sampled at *hours 1* and *2* postinfusion before the animal was removed from the aquarium and quickly killed as described above so that gill tissue could be collected for RNA processing. An additional three fish were exposed to twice the acid load (2 mmol/kg) using the same time course as above. Differences between control and postinfusion plasma pH values were analyzed by paired Student's t-tests after using the Bonferroni procedure to control for error rate for repeated-measures data (overall protection level, 0.05).

To measure gene expression, RNA was reverse transcribed as above, and the manufactured cDNA was used in triplicate samples in real-time quantitative PCR (qPCR) reactions in the presence of SYBR Green (Molecular Probes, Eugene, OR) binding dye in a Stratagene MX4000 qRT-PCR system (Stratagene, La Jolla, CA) with the following parameters: initial denaturing for 10 min at 95°C followed by 40 cycles of 35 s at 95°C, 30 s at 60°C, and 30 s at 72°C. After the final cycle, a melting curve analysis was done to verify the amplification of only one product in each well. Each sample contained 0.2 μl of cDNA (2 μl of a 1:10 dilution of stock cDNA), 7.4 pmol of each primer, and SYBR Green Master Mix (Applied Biosystems, Foster City, CA) in a total volume of 25 μl. Specific primers for NHE2 (NHE2-F3 and NHE2-B3; above), H^+-ATPase, and L8 sequence were developed (MacVector) and tested for single product production by gel electrophoresis and melting point analysis on the qPCR system. Primers for dogfish H^+-ATPase sequence (NCBI EU004205) were

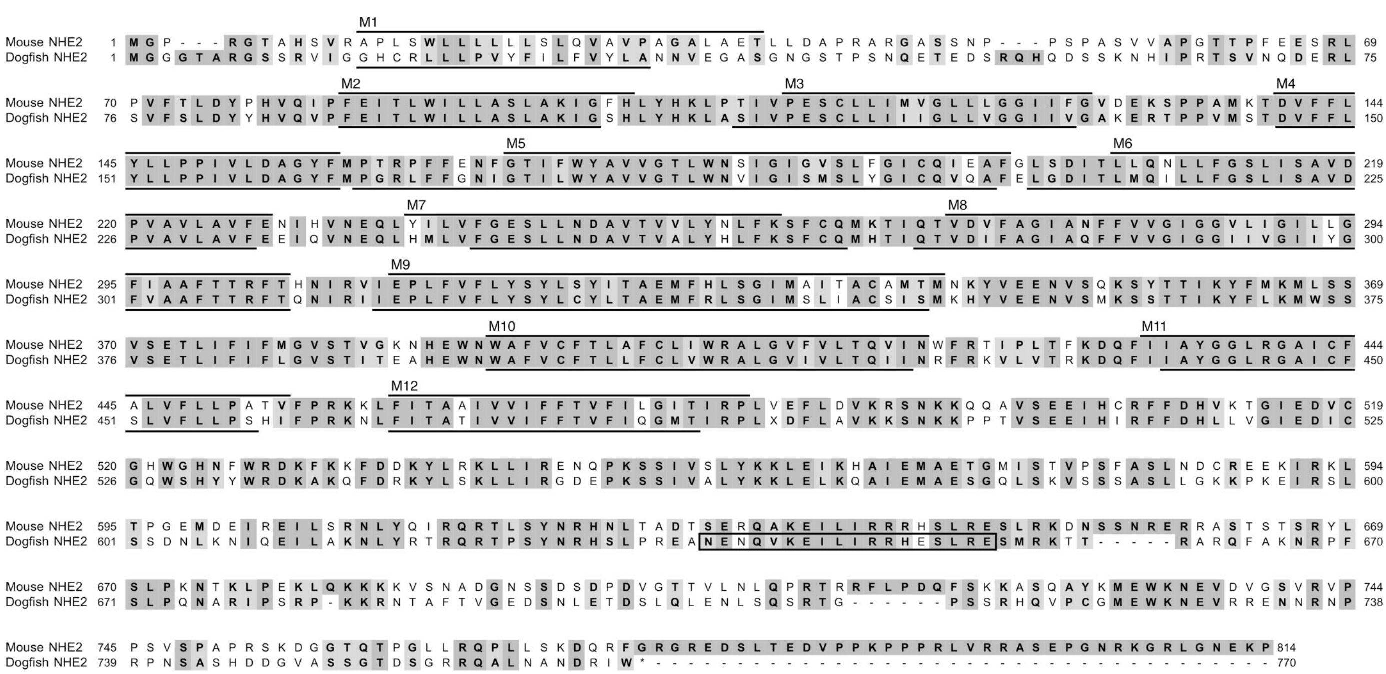

Fig. 2. Homology alignment of putative dogfish NHE2 sequence (NCBI no. DQ324545) with mouse NHE2 (NP_001028461). Dark shading represents identical amino acids, and light shading indicates functionally homologous residues. The sequences exhibit 58% identity and 70% homology overall. The epitope for the dogfish antibodies is indicated by the boxed area. Predicted transmembrane regions (1) for mouse and dogfish are shown with dark lines (M1–M12).

Downloaded from ajpregu.physiology.org on March 4, 2008

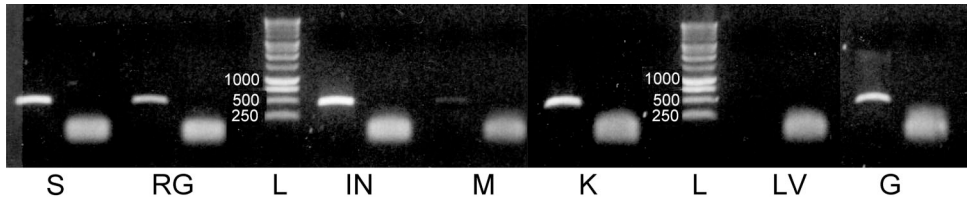

Fig. 3. RT-PCR analysis of selected dogfish tissues using NHE2 and actin specific primers. For each tissue, the first well is the NHE2 band, and the second is the actin positive control. All negative controls (containing no cDNA) were negative. The actin primers generated transcripts in all tissues tested, whereas NHE transcript was clearly detected in all epithelial tissues, including the gills. S, stomach; RG, rectal gland; L, DNA ladder; IN, intestine; M, skeletal muscle; K, kidney; LV, liver; G, gill.

HAT-F3: 5′-GGA AAC CCA TTG ACA GAG GAC C-3′ and HAT-B3: 5′-CAT TAT GTG GCA AAC CCG CTG-3′, which generated a 195-bp product. Primers (L8-F1 5′-GGA TAC ATC AAG GGA ATC GTG AAR GA-3′ & L8-B1 5′-CAG TTT CGC TTG GCC TTG TAY TTR TGR-3′) against the ribosomal protein L8 were designed by homology comparisons with published sequences, and the 470-bp L8 product from the dogfish (NCBI EU004204) was used as an internal control (12, 14). Differences in relative gene expression between control and acidotic animals were analyzed by unpaired Student's *t*-tests.

RESULTS

The predicted 770-amino acid ORF for the dogfish NHE-like sequence (NCBI no. DQ324545) showed the highest homology to NHE2 isoforms. Phylogenetic comparisons of the dogfish amino acid sequence with published vertebrate protein coding regions for NHE1–4 (Fig. 1) indicated that the dogfish NHE was most similar to mammalian NHE2 (~0.23 difference) followed by NHE4 (~0.37 difference). The dogfish sequence was also more similar to mammalian and chicken NHE2 than to teleost orthologs (mean difference from 3 species: 0.40 ± 0.07). When aligned with the mouse NHE2 sequence (NCBI AA NP_001028461; Fig. 2), the dogfish ORF was 58% identical and 70% homologous overall. The region of the dogfish sequence between residues 15-489 included 12 postulated membrane-spanning domains and was well conserved to the mouse sequence in this area (71% identity, 83% homology).

Using specific PCR primers designed from the *Squalus* NHE2 and actin sequences, we performed RT-PCR on mRNA isolated from stomach, rectal gland, intestine, skeletal muscle, kidney, liver. and gill (Fig. 3). Gel electrophoresis of the PCR products revealed that actin bands of similar densities were visible in all tissues. NHE2 primers also generated strong bands in all of the epithelial tissues tested, and a lower intensity product in skeletal muscle. No band was visible in the liver sample.

In situ hybridization detection of the mRNA in dogfish gill sections with antisense and sense NHE2 probes is shown in Fig. 4. The antisense probe labeled interlamellar cells and ovoid cells along the length of the lamellae. No binding was detected with the sense probe. This distribution was similar to that observed with NHE2 specific antibodies (Fig. 5). Cells along the filament and the base of the lamellae often exhibited light punctate staining, whereas most cells along the lamellae were strongly stained in a more diffuse cytoplasmic pattern (Fig. 5, *A*, *C*, and *D*; antibody 541-AP). In one of three dogfish tested in early trials, antibodies contained in sera from both immunized rabbits (540 and 541) recognized cells along the lamellae with a less dense and more apical specific staining pattern (Fig. 5, *E* and *F*). No staining was detected with block only or in preabsorption controls. The large immunopositive lamellar cells exhibited the strongest staining with 541-AP, and some cells in this region exhibited increased immunoreactivity near the apical edge. Western blots of gill and additional dogfish tissues probed with affinity purified antibody (540-AP; Fig. 6) and 540 serum recognized a distinct band at ~70 kDa. Strong immunolabeling was noted in gill, stomach, heart, and rectal gland, with a weaker signal in brain. No binding was observed in liver.

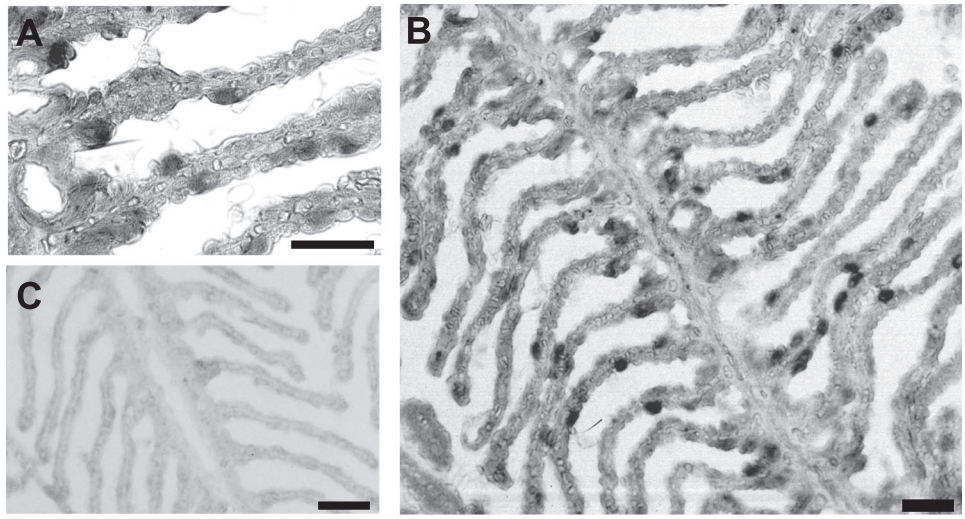

Fig. 4. In situ hybridization of dogfish specific mRNA NHE2 sequence in gill sections. *A* and *B* were hybridized with the antisense probe, whereas *C* was incubated with the sense control. Large ovoid cells along and between the lamellae expressed NHE2 mRNA. The sense probe did not hybridize to cells. Scale bars: 20 μm (*A*) and 50 μm (*B* and *C*).

Downloaded from ajpregu.physiology.org on March 4, 2008

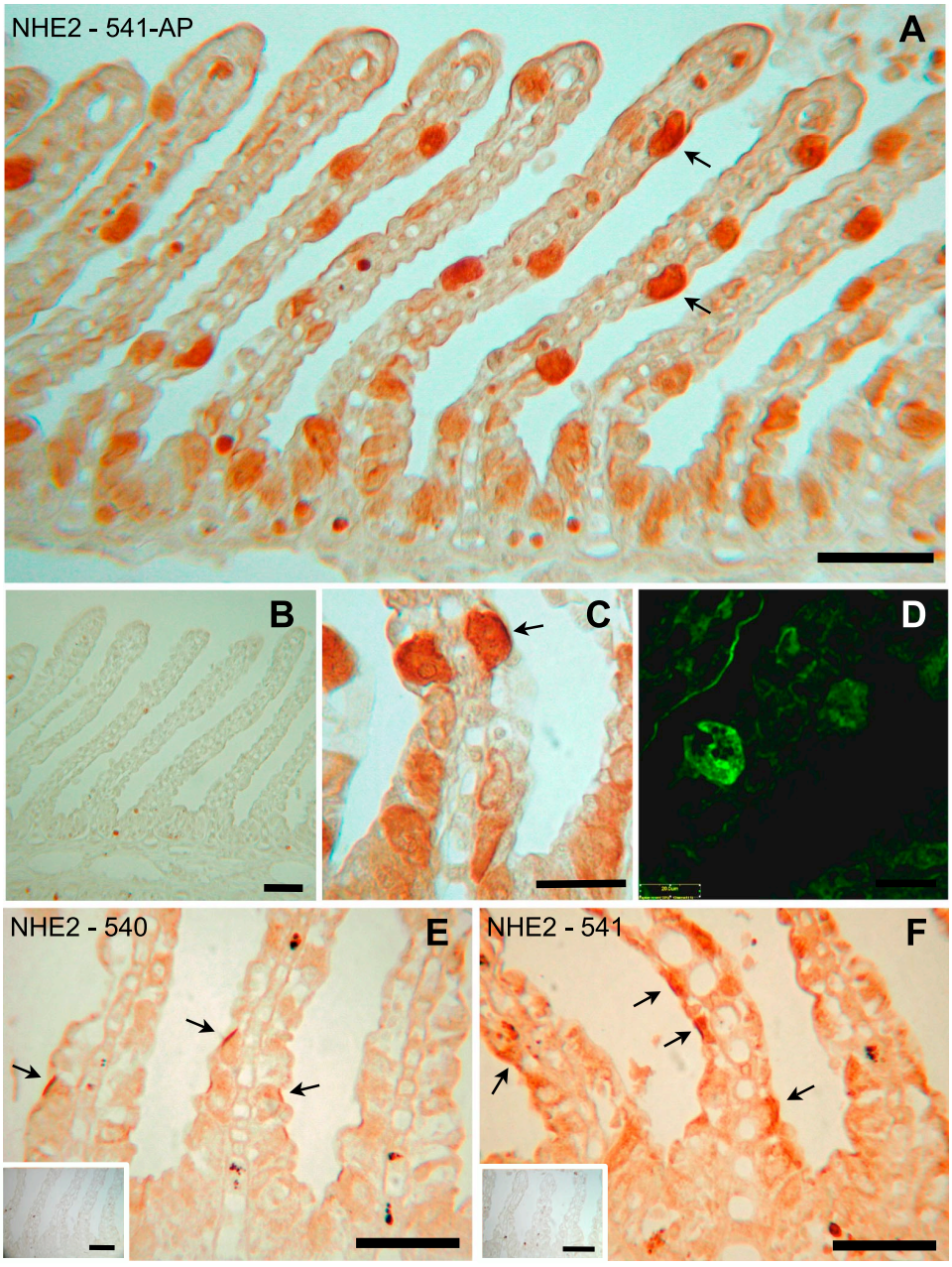

Fig. 5. Representative immunohistochemical detection with NHE2 specific antibody (541-AP; 1:750) and stained with 3,3′-diaminobenzidine tetrahydrocholride (DAB; *A*) or fluorescein (*D*) in dogfish gill sections. *A* and *C* show a dense staining pattern of cells on the lamellae and lighter staining at the base of the lamellae and in the interlamellar region on the gill filament. Some lamellar cells exhibit increased staining in the apical region (arrows). No staining is apparent in preabsorption controls (*B*). A laser confocal image (*D*) of the lamellar region shows staining that appears punctate in some cells and more broadly diffuse in others. *E* and *F* demonstrate an apical binding pattern (indicated by arrows) observed in one of three fish when plasma (1:5,000 dilution) from rabbits immunized against 540 or 541 was used (nonaffinity purified). *Insets* show negative controls (no primary antibody). Scale bars for *A*, *B*, *E*, and *F* are 50 μm and for *C* and *D* are 20 μm.

Heterologous antibodies against Na^+-K^+-ATPase and H^+-ATPase were used to identify numerous branchial cells expressing these proteins. Staining for Na^+-K^+-ATPase was often most dense along the basolateral margin of lamellar cells, whereas H^+-ATPase was both basolateral and cytoplasmic. To relate NHE2 expression, we performed colocalization with the Na^+-K^+-ATPase antibody in combination with either NHE2 (541-AP) or H^+-ATPase (Fig. 7). The large ovoid lamellar cells predominantly stained for NHE2 but not Na^+-K^+-ATPase (Fig. 7*A*), whereas other lamellar cells most positive for Na^+-K^+-ATPase had some mild NHE2 staining as well (Fig. 7*A*). Interlamellar cells had more even staining for both proteins (Fig. 7*A*). In contrast, there was little colocalization observed in sections immunolabeled with H^+-ATPase and Na^+-K^+-ATPase (Fig. 7*B*). Serial sections (10 μm) from the gills were each stained with one of the three antibodies (Fig. 8). The ovoid lamellar cells often appeared to stain for both NHE2 and H^+-ATPase (Fig. 8, *B* and *C*). Other NHE2 immunopositive cells along the lamellae coexpressed Na^+-K^+-ATPase (Fig. 8, *A* and *B*).

Animals exposed to an infusion of 1 or 2 meq/kg HCl in Ringer over 1 h exhibited a significant fall in plasma pH following the infusion that then returned to near control levels (Fig. 9*B*). Plasma pH fell from 7.81 ± 0.04 to 7.62 ± 0.07 (1 meq acid group; mean ± SE, $n = 5$, $P < 0.05$) and from 7.86 ± 0.02 to 7.29 ± 0.08 (2 meq group; $n = 3$, $P < 0.05$) measured at the end of the infusion period. A control group of Ringer-infused animals did not change (7.77 ± 0.03 vs. 7.80 ± 0.01 1 h postinfusion; $n = 5$, not significant). Relative expression of message for both transporters at *hour 2* postinfusion (as measured by real-time qPCR) did not change significantly between Ringer and acid-infused groups (Fig. 9*A*).

Downloaded from ajpregu.physiology.org on March 4, 2008

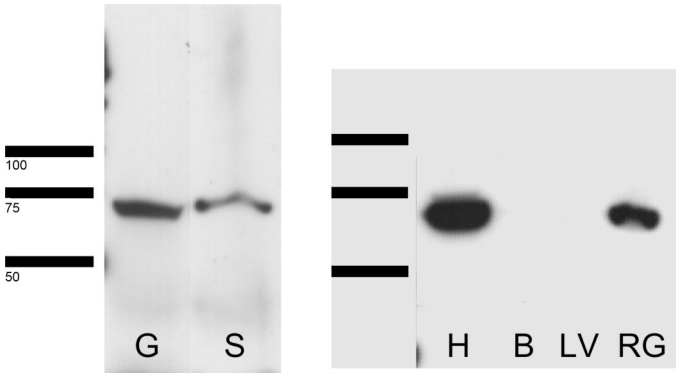

Fig. 6. Western blots of dogfish tissues probed with anti-NHE2 antibodies (540-AP). A ~70- to 72-kDa signal was detected in gill, stomach, heart, and rectal gland. Longer exposure times also showed a weaker signal in brain. Total protein (~70 μg) was loaded in each lane. Plasma containing antibody 540 also revealed bands of ~70 kDa, but immunolabeling was not detected in controls made with preimmune serum or lacking primary antibody (data not shown). Standards indicate 100, 75, and 50 kDa. H, heart; B, brain.

DISCUSSION

The dogfish gill NHE sequence exhibited 70% homology with mouse NHE2 with similar topology and putative membrane spanning regions (42). The ORF was truncated by ~39 residues at the 3′ end when compared with the mouse (Fig. 2). The dogfish sequence included a leucine at position 144 (equivalent to Leu^{143} in rabbit NHE2) that is thought to play a critical role in NHE2 amiloride sensitivity (71). Likewise, a postulated mammalian proline-rich motif involved with targeting of NHE2 to the apical surface [e.g., mouse 744–751: PPSVSPAP; (15)] has two proline residues that correspond in the dogfish region 738–740. NHE2 expression in PS-120 membranes following cell acidification also appears to require a response element located within the first 551 amino acids of the rat NHE2 sequence (29), and this area is well conserved (81% homology) between the dogfish and rat (as in mouse) NHE2. Phylogenetic analysis groups the dogfish sequence closest to mammalian NHE2 and NHE4, with NHE3 and NHE1 on separate out branches (Fig. 1). Interestingly, the dogfish sequence groups are closer to avian and mammalian NHE2 than to those described for teleost (Actinopterygii) species. This is in contrast to the generally accepted view of cartilaginous fishes being basal to other jawed vertebrates (36), although some analyses have disagreed with this model (2). This same relationship with mammalian orthologs has been described for the stingray NHE3 (12) and other transporter sequences from the dogfish (31). Data from the genome sequence of a cartilaginous species (the elephant shark, *Callorhinchus milii*) has recently demonstrated that the human and shark genome exhibit a higher level of sequence conservation than is found between humans and teleosts (61, 62). These differences are likely because of the rapid divergence of the teleosts, since this group is thought to have gone through one or more additional genome duplications after their split from the tetrapod line (16).

As noted by Brett and coworkers (5), mammalian NHE2 and NHE4 are located adjacent to each other on the same chromosome (in humans, 2q11) and likely arose from a recent gene duplication. To date, NHE4 has not been found in a fish genome or from the cloning of full-length cDNA for eight members of the NHE family in *Danio rerio* (69), giving support to the suggestion that this isoform arose after the tetrapod line diverged from fishes (12). It is feasible that the dogfish NHE2 (and NHE2/4 in fishes in general) could carry out functions ascribed to both NHE2 and NHE4 in mammals (see below).

mRNA and protein expression for dogfish NHE2 (as detected by RT-PCR and Western blotting; Figs. 3 and 6) were detected in a variety of transporting tissues (gill, rectal gland, stomach, intestine, and kidney) and also heart, with a weaker signal in muscle and brain. In mammals, NHE2 message has been found predominantly in kidney, intestine, stomach (in rat; 64); kidney, intestine, and adrenal gland with lower expression in skeletal muscle and trachea (in rabbit; 60); and colon, kidney, and skeletal muscle (in humans; 39). The dogfish antibody recognized a protein of ~70 kDa in the Western blots that was slightly smaller in size to that reported in rat, mouse,

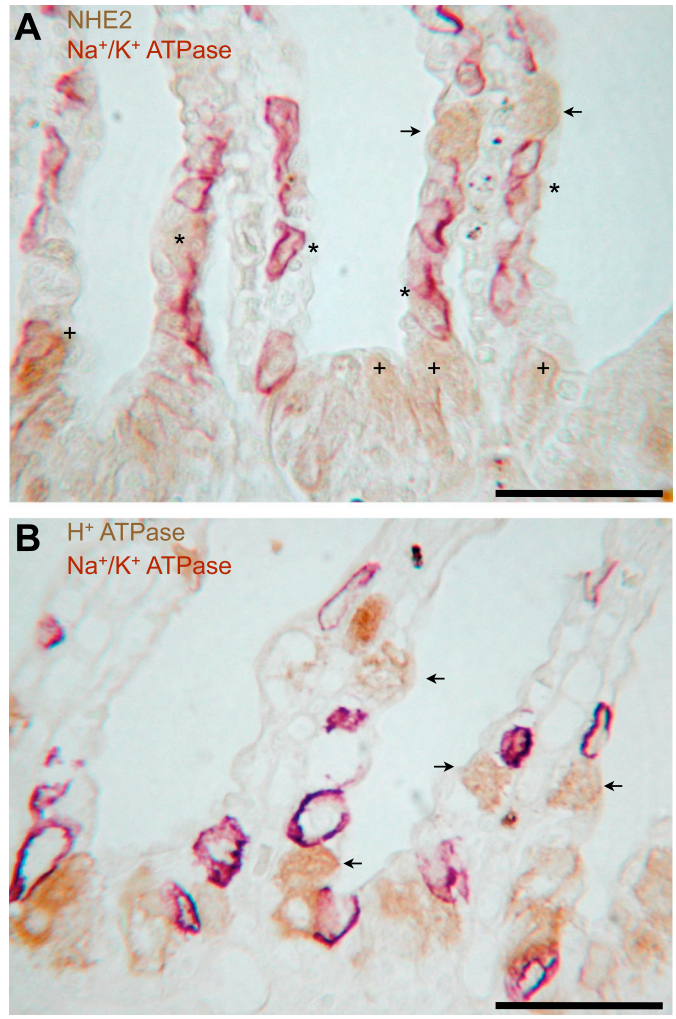

Fig. 7. Colocalization of NHE2 (541-AP; brown) with Na^+-K^+ ATPase (purple; *A*) and H^+-ATPase (brown) with Na^+-K^+-ATPase (purple; *B*). Cells along the base of the lamellae showed mild labeling for both NHE and Na^+-K^+ ATPase (+). Cells predominantly immunopositive for Na^+-K^+-ATPase on the lamellae also had some NHE expression (*). Some large ovoid cells on the lamellae also stained for NHE with little or no Na^+-K^+-ATPase (arrows). There was little overlap between cells staining for H^+-ATPase and Na^+-K^+-ATPase. Many of the lamellar H^+-ATPase-expressing cells were also ovoid (arrows). Scale bars are 50 μm.

Downloaded from ajpregu.physiology.org on March 4, 2008

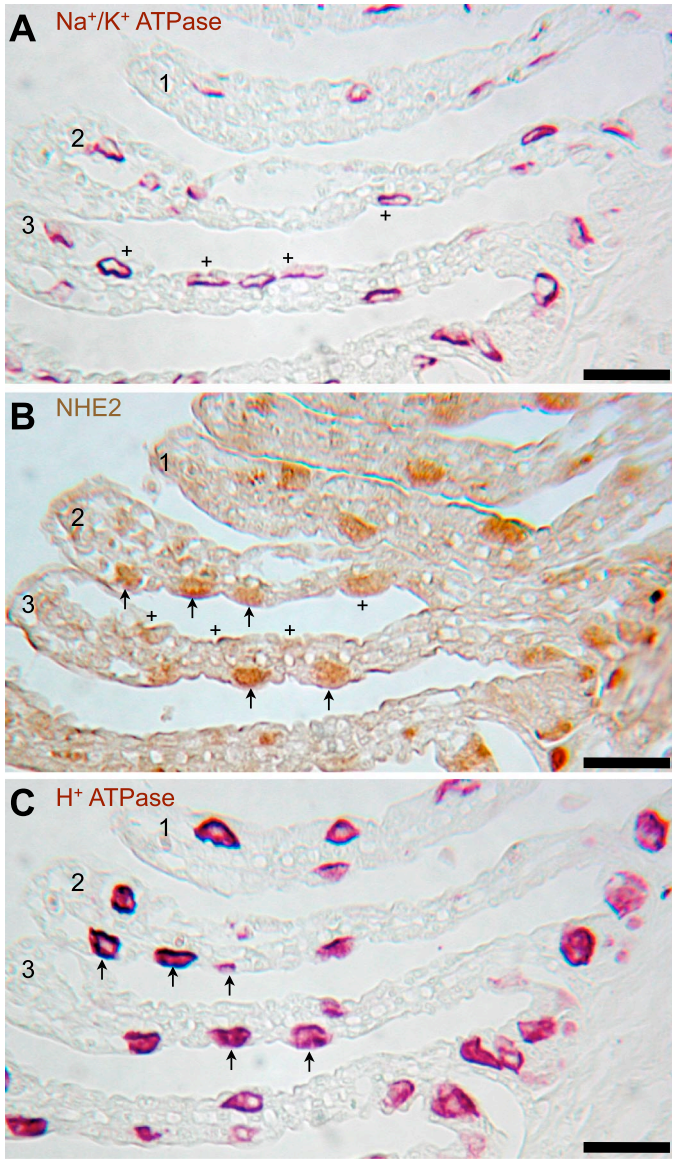

Fig. 8. Representative 10-μm serial sections from dogfish gill, labeled for Na^+-K^+-ATPase (*A*), NHE2 with 541-AP (*B*), and H^+-ATPase (*C*). Nos. indicate corresponding lamellae. Cells immunolabeled with Na^+-K^+-ATPase often exhibited mild staining for NHE2 but not H^+-ATPase (+). In contrast, another population of cells in the lamellae stained for both NHE2 and H^+-ATPase but not Na^+-K^+-ATPase (arrows). Staining with DAB (*B*) and vasoactive intestinal peptide (*A* and *C*). Scale bars are 50 μm.

or expressed in PS-120 cells (range from <90 to 75 kDa; see Refs. 4, 52, and 59). A putative teleost NHE2 (measured with a species-specific antibody) was ~85 kDa (6). An antibody against rabbit NHE2 used on immunoblots of dogfish gill proteins recognized a protein at ~80 kDa (56). It should be noted that the final 87 amino acids of the rabbit NHE2 sequence used to make this polyclonal antibody (59) share 22 identical and 14 similar residues distributed over the length of a 135-residue region of the 3′ end in the dogfish sequence described in the present study. Thus it is unclear whether these earlier immunological results show cross reactivity with the same protein that we have identified as NHE2 here.

Gill cells both along the lamellae and within the interlamellar region were labeled by the antisense mRNA probe for the dogfish NHE2 (Fig. 4). The darkest staining for cells expressing NHE2 mRNA was predominantly in large ovoid cells on the lamellae. Immunodetection with dogfish specific antibodies (Fig. 5) revealed a similar pattern with a strong reaction in the ovoid lamellar cells and a lighter staining in columnar- or squamous-shaped cells at the base of and between the lamellae. In these cells, and one of three animals tested with the anti-NHE2 immune serum, the immunolocalization of the NHE2 was along the apical edge or more diffuse in the cytoplasm (Fig. 5). The two different cell morphologies apparent in the dark- and light-staining cells are suggestive of two distinct cell types with differential NHE2 expression. Lending credence to this suggestion are the localizations of H^+-ATPase and Na^+-K^+-ATPase in relation to the NHE2 (Figs. 7 and 8). The H^+-ATPase appears throughout the cell with strong staining along the basolateral margins. Serial gill sections stained with the NHE2 and H^+-ATPase antibodies indicate that the two

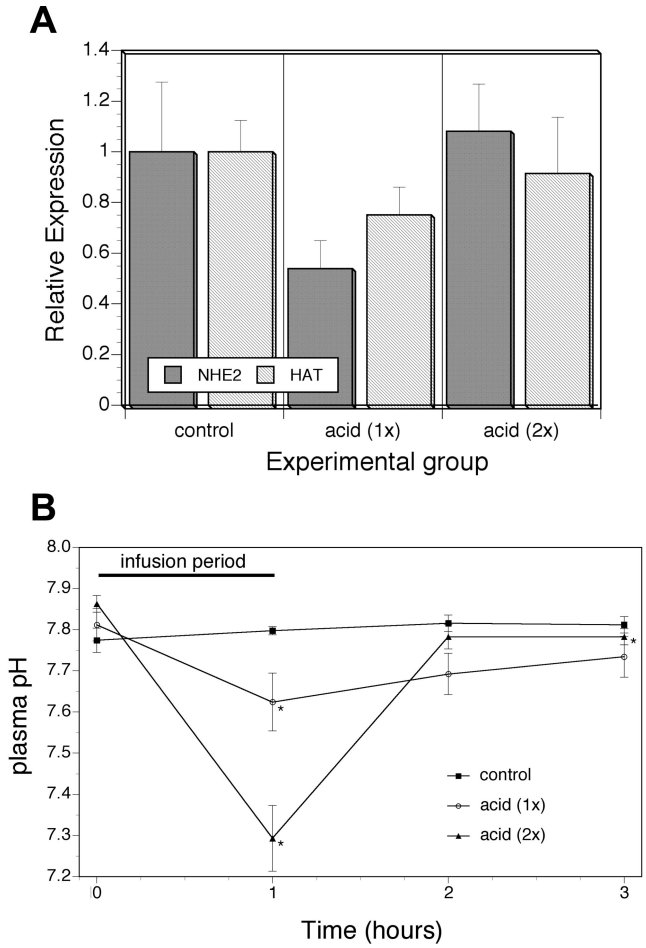

Fig. 9. Real-time quantitative PCR analysis (*A*) of NHE2 and H^+-ATPase mRNA expression in dogfish 2 h after an infused acid load (1 or 2 mmol/kg given over a 1-h period via the dorsal aorta). Relative expression is normalized to the level of ribosomal protein L8 mRNA, and control values are set to a relative expression level of 1.0. No significant change was noted in the mRNA levels of either NHE or H^+-ATPase message. Doubling the acid load in a second group of fish (2× group) induced a higher level of NHE2 expression, but the change was not significant. *B*: plasma pH change before and following the infusion. *Significant change in plasma pH (n = 5 for control and 1× acid-infused groups, n = 3 for 2× acid group; means ± SE). Gills for RT-PCR shown in *A* were collected immediately following the *hour 3* blood pH measurement.

Downloaded from ajpregu.physiology.org on March 4, 2008

proteins are often colocalized in the ovoid lamellar cells. In contrast, H^+-ATPase and Na^+-K^+-ATPase do not appear in the same cells. In the Na^+-K^+-ATPase-expressing cells, the labeling is basolateral with NHE2 sometimes colocalized in apical or cytoplasmic regions of these cells (Fig. 8, *A* vs. *B*).

Piermarini et al. (48) showed that gill cells in the Atlantic stingray that reacted strongly for antibodies against basolateral H^+-ATPase also exhibited apical immunolabeling with antibodies for pendrin Cl^-/HCO_3^- exchanger. They postulated that these were base-excreting cells analogous to the B type intercalated cells of mammalian renal tubule. The dogfish also exhibits the same distribution of pendrin in H^+-ATPase cells (25). Tresguerres and coworkers (56–58) have shown that these cells in dogfish respond to metabolic alkalosis by translocating intracellular H^+-ATPase to the basolateral margins and postulated that this drives proton reabsorption (and presumably HCO_3^- excretion). They also found an increase in NHE2 protein expression via Western blots following acid infusion, but immunolocalization was not successful (56). Edwards (21) reported colocalization of NHE2 and Na^+-K^+-ATPase in the gills of three elasmobranch species. Both of these studies utilized the heterologous antibody against rabbit NHE2 (with the caveats noted above). The present results demonstrate the colocalization of NHE2 and Na^+-K^+-ATPase in some branchial cells, and a novel location for NHE2 in the putative base-excreting (H^+-ATPase-expressing) cells. It is likely that the NHE2 found with Na^+-K^+-ATPase is involved with apical Na^+ uptake and H^+ excretion to the environment in a fashion similar to proximal tubular mammalian NHE2 and perhaps as a complement to apical NHE3 (see below). We speculate that the predominant expression of NHE2 in the H^+-ATPase-rich cells may also assist with regulation of pH_i and basolateral H^+ reabsorption in parallel to H^+-ATPase pumping (driving apical base excretion) in a fashion analogous to NHE4 in the mammalian nephron (9, 45) and pancreas (49). Basolateral NHE2 is also thought to regulate pH_i in acid-secreting parietal cells of mammalian gastric mucosa (50). It remains to be seen if the cytoplasmic NHE2 expression in these cells shifts to a more basolateral orientation during the postprandial period in parallel to the movement of H^+-ATPase. (58, 67).

Acid infusions induced the expected metabolic acidosis and recovery (20), but significant changes in mRNA for NHE2 and H^+-ATPase were not detected. Gill samples were collected 2 h postinfusion, at a time when peak acid excretion following infusion is beginning (53). If NHE2, located in two different cell types (as above), is involved in responses to both acidosis and alkalosis, it is feasible that net NHE2 mRNA levels would show little change, since the message is upregulated in one cell type but downregulated in the other in response to acidosis. Posttranslational mechanisms such as changes to membrane cycling of NHE2 (7) or protein phosphorylation (38) could be responsible for short-term adjustments. For example, mammalian NHE2 expressed in NHE-deficient PS-120 cells has a plasma membrane half-life of ~3 h (8). Gens et al. (29) showed that fusion protein constructs of rat NHE2 expressed in PS-120 cells are responsive to decreased pH_i, since more NHE is shuttled to the membrane following cell acidification. Thus cycling of NHE2 between membrane and intracellular compartments in the dogfish following systemic acidosis would allow adjustments at the protein level in the time course measured here. It remains to be seen if increased NHE2 mRNA transcription (and subsequent de novo protein expression) may occur in longer-term acid (or alkaline) exposure. It is also likely that apically expressed branchial NHE3, which is colocalized in Na^+-K^+-ATPase cells (10), plays an important role in the overall adjustments to acid challenge. Both isoforms function in Na^+ uptake in the mouse colon (30), and NHE2 could act as a "backup" during acidosis as observed in the proximal tubule of NHE3-deficient mice (3).

Perspectives and Significance

NHE2 is thought to have first appeared in fishes (5), and we have shown here that the dogfish expresses an NHE2 that is similar to mammalian homologs. Chondrichthyan fishes are thought to have evolved ~450 million years ago (40), so this ortholog appears to have been well conserved through the vertebrate lineage. The protein may play a role in acid and/or base transfers across the dogfish gill and is found in multiple branchial cell types. NHE2 is also present in other dogfish tissues such as the stomach, intestine, and rectal gland, implying osmoregulatory roles for this transporter as well.

GRANTS

This research was supported by National Science Foundation Grants IBN-0111073 and IOB-0616187 to J. B. Claiborne, IBN-0089943 to D. H. Evans, and 0413427 to K. P. Choe and by Mount Desert Island Biological Laboratory New Investigator Award to S. L. Edwards.

REFERENCES

1. **Argos P, Rao JK, Hargrave PA.** Structural prediction of membrane-bound proteins. *Eur J Biochem* 128: 565–575, 1982.
2. **Arnason U, Gullberg A, Janke A, Joss J, Elmerot C.** Mitogenomic analyses of deep gnathostome divergences: a fish is a fish. *Gene* 333: 61–70, 2004.
3. **Bailey MA, Giebisch G, Abbiati T, Aronson PS, Gawenis LR, Shull GE, Wang T.** NHE2-mediated bicarbonate reabsorption in the distal tubule of NHE3 null mice. *J Physiol* 561: 765–775, 2004.
4. **Bookstein C, Xie Y, Rabenau K, Musch MW, McSwine RL, Rao MC, Chang EB.** Tissue distribution of Na^+/H^+ exchanger isoforms NHE2 and NHE4 in rat intestine and kidney. *Am J Physiol Cell Physiol* 273: C1496–C1505, 1997.
5. **Brett CL, Donowitz M, Rao R.** Evolutionary origins of eukaryotic sodium/proton exchangers. *Am J Physiol Cell Physiol* 288: C223–C239, 2005.
6. **Catches JS, Burns JM, Edwards SL, Claiborne JB.** Na^+/H^+ antiporter (NHE2), V-H^+-ATPase, and Na^+/K^+-ATPase immunolocalization in a marine teleost (*Myoxocephalus octodecimspinosus*). *J Exp Biol* 209: 3440–3447, 2006.
7. **Cavet ME, Akhter S, De Medina FS, Donowitz M, Tse CM.** Na^+/H^+ exchangers (NHE1-3) have similar turnover numbers but different percentages on the cell surface. *Am J Physiol Cell Physiol* 277: C1111–C1121, 1999.
8. **Cavet ME, Akhter S, Murtazina R, De Medina FS, Tse CM, Donowitz M.** Half-lives of plasma membrane Na^+/H^+ exchangers NHE1-3: plasma membrane NHE2 has a rapid rate of degradation. *Am J Physiol Cell Physiol* 281: C2039–C2048, 2001.
9. **Chambrey R, St John PL, Eladari D, Quentin F, Warnock DG, Abrahamson DR, Podevin RA, Paillard M.** Localization and functional characterization of Na^+/H^+ exchanger isoform NHE4 in rat thick ascending limbs. *Am J Physiol Renal Physiol* 281: F707–F717, 2001.
10. **Choe K, Edwards S, Claiborne J, Evans D.** The putative mechanism of Na(+) absorption in euryhaline elasmobranchs exists in the gills of a stenohaline marine elasmobranch, *Squalus acanthias. Comp Biochem Physiol A Mol Integr Physiol* 146: 155–162, 2007.
11. **Choe KP, Edwards S, Morrison-Shetlar A, Toop T, Claiborne JB.** Immunolocalization of Na^+/K^+-ATPase in mitochondrion-rich cells of the atlantic hagfish (*Myxine glutinosa*) gill. *Comp Biochem Physiol* 124: 161–168, 1999.

Downloaded from ajpregu.physiology.org on March 4, 2008

12. **Choe KP, Kato A, Hirose S, Plata C, Sindic A, Romero MF, Claiborne JB, Evans DH.** NHE3 in an ancestral vertebrate: primary sequence, distribution, localization, and function in gills. *Am J Physiol Regul Integr Comp Physiol* 289: R1520–R1534, 2005.
13. **Choe KP, Morrison-Shetlar AI, Wall BP, Claiborne JB.** Immunological Detection of Na^+/H^+ exchangers in the gills of a hagfish, *Myxine glutinosa*, an elasmobranch, *Raja erinacea*, and a teleost, *Fundulus heteroclitus*. *Comp Biochem Physiol* 131: 375–385, 2002.
14. **Choe KP, Verlander JW, Wingo CS, Evans DH.** A putative H^+-K^+-ATPase in the Atlantic stingray, *Dasyatis sabina*: primary sequence and expression in gills. *Am J Physiol Regul Integr Comp Physiol* 287: R981–R991, 2004.
15. **Chow CW, Woodside M, Demaurex N, Yu FH, Plant P, Rotin D, Grinstein S, Orlowski J.** Proline-rich motifs of the Na^+/H^+ exchanger 2 isoform: binding of Src homology domain 3 and role in apical targeting in epithelia. *J Biol Chem* 274: 10481–10488, 1999.
16. **Christoffels A, Koh EG, Chia JM, Brenner S, Aparicio S, Venkatesh B.** *Fugu* genome analysis provides evidence for a whole-genome duplication early during the evolution of ray-finned fishes. *Mol Biol Evol* 21: 1146–1151, 2004.
17. **Claiborne JB.** Acid-Base Regulation. In: *The Physiology of Fishes* (2nd ed.), edited by Evans DH. Boca Raton, FL: CRC, 1998, p. 179–200.
18. **Claiborne JB, Blackston CR, Choe KP, Dawson DC, Harris SP, MacKenzie LA, Morrison-Shetlar AI.** A mechanism for branchial acid excretion in marine fish: identification of multiple Na^+/H^+ antiporter isoforms (NHE) in gills of two seawater teleosts. *J Exp Biol* 202: 315–324, 1999.
19. **Claiborne JB, Edwards SL, Morrison-Shetlar AI.** Acid-base regulation In fishes: cellular and molecular mechanisms. *J Exp Zool* 293: 302–319, 2002.
20. **Claiborne JB, Evans DH.** Acid-base balance and ion transfers in the spiny dogfish (*Squalus acanthias*) during hypercapnia: a role for ammonia excretion. *J Exp Zool* 261: 9–17, 1992.
21. **Edwards SL, Donald JA, Toop T, Donowitz M, Tse CM.** NHE-like immunoreactivity in the gills of elasmobranchs. *Comp Biochem Physiol* 131: 257–265, 2002.
22. **Evans DH.** Mechanisms of acid extrusion by two marine fishes: the teleost, *Opsanus beta*, and the elasmobranch, *Squalus acanthias*. *J Exp Biol* 97: 289–299, 1982.
23. **Evans DH.** The roles of gill permeability and transport mechanisms in euryhalinity. In: *Fish Physiology*, edited by Hoar WS and Randall DJ. New York: Academic, 1984, p. 239–283.
24. **Evans DH, Kormanik GA, Krasny EJ Jr.** Mechanisms of ammonia and acid extrusion by the little skate, *Raja erinacea*. *J Exp Zool* 208: 431–437, 1979.
25. **Evans DH, Piermarini PM, Choe KP.** Homeostasis: osmoregulation, pH regulation, and nitrogen excretion. In: *Biology of Sharks and their Relatives*, edited by Carrier JC, Musick JA, and Heithaus MR. Boca Raton, FL: CRC, 2004, p. 247–268.
26. **Evans DH, Piermarini PM, Choe KP.** The multifunctional fish gill: dominant site of gas exchange, osmoregulation, acid-base regulation, and excretion of nitrogenous waste. *Physiol Rev* 85: 97–177, 2005.
27. **Filippova M, Ross LS, Gill SS.** Cloning of the V-ATPase B subunit cDNA from Culex quinquefasciatus and expression of the B and C subunits in mosquitoes. *Insect Mol Biol* 7: 223–232, 1998.
28. **Forster RP, Goldstein L, Rosen JK.** Intrarenal control of urea reabsorption by renal tubules of the marine elasmobranch, *Squalus acanthias*. *Comp Biochem Physiol A* 42: 3–12, 1972.
29. **Gens JS, Du H, Tackett L, Kong SS, Chu S, Montrose MH.** Different ionic conditions prompt NHE2 and NHE3 translocation to the plasma membrane. *Biochim Biophys Acta* 1768: 1023–1035, 2007.
30. **Guan Y, Dong J, Tackett L, Meyer J, Shull G, Montrose M.** NHE2 is the main apical NHE in mouse colonic crypts but an alternative Na^+-dependent acid extrusion mechanism is upregulated in NHE2-null mice. *Am J Physiol Gastrointest Liver Physiol* 291: G689–G699, 2006.
31. **Harmel N, Djurisic M, Forbush B.** The placement of Chondrichthyes within the vertebrate phylogenetic tree. *Bull Mt Desert Is Biol Lab* 45: 53–54, 2006.
32. **Heisler N.** Acid-base regulation in fishes. In: *Fish Physiology*, edited by Hoar WS and Randall DJ. New York: Academic, 1984, p. 315–401.
33. **Heisler N.** Acid-base Regulation in Fishes. In: *Acid-Base Regulation in Animals*, edited by Heisler N. Amsterdam: Elsvier, 1986, p. 309–356.
34. **Heisler N, Toews D, Holeton G.** Regulation of ventilation and acid-base status in the elasmobranch *Scyliorhinus stellaris* during hyperoxia-induced hypercapnia. *Respir Physiol* 71: 227–246, 1988.
35. **Hirata T, Kaneko T, Ono T, Nakazato T, Furukawa N, Hasegawa S, Wakabayashi S, Shigekawa M, Chang MH, Romero MF, Hirose S.** Mechanism of acid adaptation of a fish living in a pH 3.5 *lake Am J Physiol Regul Integr Comp Physiol* 284: R1199–R1212, 2003.
36. **Kikugawa K, Katoh K, Kuraku S, Sakurai H, Ishida O, Iwabe N, Miyata T.** Basal jawed vertebrate phylogeny inferred from multiple nuclear DNA-coded genes (Abstract). *BMC Biol* 2: 3, 2004.
37. **Kormanik GA, Wilkins T, Banks J.** Proton-transporting ATPase activity in crude homegenates of gill tissue from the little skate, *Raja erinacea*. *Bull Mt Desert Island biol Lab* 36: 60–62, 1997.
38. **Levine SA, Montrose MH, Tse CM, Donowitz M.** Kinetics and regulation of three cloned mammalian Na^+/H^+ exchangers stably expressed in a fibroblast cell line. *J Biol Chem* 268: 25527–25535, 1993.
39. **Malakooti J, Dahdal RY, Schmidt L, Layden TJ, Dudeja PK, Ramaswamy K.** Molecular cloning, tissue distribution, and functional expression of the human Na^+/H^+ exchanger NHE2. *Am J Physiol Gastrointest Liver Physiol* 277: G383–G390, 1999.
40. **Miller RF, Cloutier R, Turner S.** The oldest articulated chondrichthyan from the Early Devonian period. *Nature* 425: 501–504, 2003.
41. **Murdaugh HV, Robin ED.** Acid-base metabolism in the dogfish shark. In: *Sharks, Skates and Rays*, edited by Gilbert PW, Mathewson RF, and Rall DR. Baltimore, MD: Johns Hopkins, 1967, p. 249–264.
42. **Noel J, Pouyssegur J.** Hormonal regulation, pharmacology, and membrane sorting of vertebrate Na^+/H^+ exchanger isoforms. *Am J Physiol Cell Physiol* 268: C283–C296, 1995.
43. **Paillard M.** Na^+/H^+ exchanger subtypes in the renal tubule: function and regulation in physiology and disease. *Exp Nephrol* 5: 277–284, 1997.
44. **Perry SF, Gilmour KM.** Acid-base balance and CO_2 excretion in fish: Unanswered questions and emerging models. *Respir Physiol Neurobiol* 154: 199–215, 2006.
45. **Peti-Peterdi J, Chambrey R, Bebok Z, Biemesderfer D, St John PL, Abrahamson DR, Warnock DG, Bell PD.** Macula densa Na^+/H^+ exchange activities mediated by apical NHE2 and basolateral NHE4 isoforms. *Am J Physiol Renal Physiol* 278: F452–F463, 2000.
46. **Piermarini P, Evans DH.** Effects of environmental salinity on Na^+/K^+-ATPase in the gills and rectal gland of a euryhaline elasmobranch (*Dasyatis sabina*). *J Exp Biol* 203: 2957–2966, 2000.
47. **Piermarini PM, Evans DH.** Immunochemical analysis of the vacuolar-proton-ATPase B-subunit in the gills of a euryhaline stingray (*Dasyatis sabina*): effects of salinity and realation to Na^+/K^+-ATPase. *J Exp Biol* 204: 3251–3259, 2001.
48. **Piermarini PM, Verlander JW, Royaux IE, Evans DH.** Pendrin immunoreactivity in the gill epithelium of a euryhaline elasmobranch. *Am J Physiol Regul Integr Comp Physiol* 283: R983–R992, 2002.
49. **Roussa E, Alper SL, Thevenod F.** Immunolocalization of anion exchanger AE2, Na^+/H^+ exchangers NHE1 and NHE4, and vacuolar type H^+-ATPase in rat pancreas. *J Histochem Cytochem* 49: 463–474, 2001.
50. **Schultheis P, Clarke L, Meneton P, Harline M, Boivin G, Stemmermann G, Duffy J, Doetschman T, Miller M, Shull G.** Targeted disruption of the murine Na^+/H^+ exchanger isoform 2 gene causes reduced viability of gastric parietal cells and loss of net acid secretion. *J Clin Invest* 101: 1243–1253, 1998.
51. **Schuster VL.** Function and regulation of collecting duct intercalated cells. *An Rev Physiol* 55: 267–288, 1993.
52. **Sun AM, Liu Y, Dworkin LD, Tse CM, Donowitz M, Yip KP.** Na^+/H^+ exchanger isoform 2 (NHE2) is expressed in the apical membrane of the medullary thick ascending limb. *J Membr Biol* 160: 85–90, 1997.
53. **Swenson ER, Fine AD, Maren TH.** Effects of H^+/K^+ ATPase inhibition on renal and branchial acid-base metabolism in the dogfish shark, *Squalus acanthias*. *Bull Mt Desert Is Biol Lab* 32: 89–91, 1993.
54. **Swenson ER, Maren TH.** The roles of gill and red cell carbonic anhydrase in elasmobranch HCO_3^- and CO_2 excretion. *Am J Physiol Regul Integr Comp Physiol* 253: R450–R458, 1987.
55. **Towle D, Rushton M, Heidysch D, Magnani J, Rose M, Amstutz A, Jordan M, Shearer D, Wu W.** Sodium/proton antiporter in the euryhaline crab *Carcinus maenas*: molecular cloning, expression and tissue distribution. *J Exp Biol* 200: 1003–1014, 1997.
56. **Tresguerres M, Katoh F, Fenton H, Jasinska E, Goss GG.** Regulation of branchial V-H^+-ATPase, Na^+/K^+-ATPase and NHE2 in response to acid and base infusions in the Pacific spiny dogfish (*Squalus acanthias*). *J Exp Biol* 208: 345–354, 2005.

Downloaded from ajpregu.physiology.org on March 4, 2008

57. **Tresguerres M, Parks SK, Katoh F, Goss GG.** Microtubule-dependent relocation of branchial V-H^+-ATPase to the basolateral membrane in the Pacific spiny dogfish (*Squalus acanthias*): a role in base secretion. *J Exp Biol* 209: 599–609, 2006.
58. **Tresguerres M, Parks SK, Wood CM, Goss GG.** V-H^+-ATPase translocation during blood alkalosis in dogfish gills: interaction with carbonic anhydrase and involvement in the post-feeding alkaline tide. *Am J Physiol Regul Integr Comp Physiol* 292: R2012–R2019, 2007.
59. **Tse CM, Levine SA, Yun CH, Khurana S, Donowitz M.** Na^+/H^+ exchanger-2 is an O-linked but not an N-linked sialoglycoprotein. *Biochemistry* 33: 12954–12961, 1994.
60. **Tse CM, Levine SA, Yun CH, Montrose MH, Little PJ, Pouyssegur J, Donowitz M.** Cloning and expression of a rabbit cDNA encoding a serum-activated ethylisopropylamiloride-resistant epithelial Na^+/H^+ exchanger isoform (NHE-2). *J Biol Chem* 268: 11917–11924, 1993.
61. **Venkatesh B, Kirkness EF, Loh YH, Halpern AL, Lee AP, Johnson J, Dandona N, Viswanathan LD, Tay A, Venter JC, Strausberg RL, Brenner S.** Survey sequencing and comparative analysis of the elephant shark (*Callorhinchus milii*) genome (Abstract). *PLoS Biol* 5: e101, 2007.
62. **Venkatesh B, Tay A, Dandona N, Patil JG, Brenner S.** A compact cartilaginous fish model genome. *Curr Biol* 15: R82–R83, 2005.
63. **Wang T, Hropot M, Aronson PS, Giebisch G.** Role of NHE isoforms in mediating bicarbonate reabsorption along the nephron. *Am J Physiol Renal Physiol* 281: F1117–F1122, 2001.
64. **Wang Z, Orlowski J, Shull G.** Primary structure and functional expression of a novel gastrointestinal isoform of the rat Na/H exchanger. *J Biol Chem* 268: 11925–11928, 1993.
65. **Wilson J, Randall D, Vogl A, Iwama G.** Immunolocalization of proton-ATPase in the gills of the elasmobranch, *Squalus acanthias*. *J Exp Zool* 278: 78–86, 1997.
66. **Wilson JM, Randall DJ, Donowitz M, Vogl AW, Ip AKY.** Immunolocalization of ion transport proteins to the branchial epithelium mitochondria-rich cells in the mudskipper (*Periophthalmodon schlosseri*). *J Exp Biol* 203: 2297–2310, 2000.
67. **Wood CM, Kajimura M, Bucking C, Walsh PJ.** Osmoregulation, ionoregulation and acid-base regulation by the gastrointestinal tract after feeding in the elasmobranch (Squalus acanthias). *J Exp Biol* 210: 1335–1349, 2007.
68. **Wu M, Biemesderfer D, Giebisch G, Aronson P.** Role of NHE3 in mediating renal brush border Na^+-H^+ exchange. Adaptation to metabolic acidosis. *J Biol Chem* 271: 32749–32752, 1996.
69. **Yan JJ, Chou MY, Kaneko T, Hwang PP.** Gene expression of Na^+/H^+ exchanger in zebrafish H^+-ATPase-rich cells during acclimation to low-Na^+ and acidic environments. *Am J Physiol Cell Physiol* 293: C1539–C1550, 2007.
70. **Yun C, Tse C, Nath S, Levine S, Brant S, Donowitz M.** Mammalian Na^+/H^+ exchanger gene family: structure and function studies. *Am J Physiol Gastrointest Liver Physiol* 269: G1–G11, 1995.
71. **Yun CH, Little PJ, Nath SK, Levine SA, Pouyssegur J, Tse CM, Donowitz M.** Leu143 in the putative fourth membrane spanning domain is critical for amiloride inhibition of an epithelial Na^+/H^+ exchanger isoform (NHE-2). *Biochem Biophys Res Commun* 193: 532–539, 1993.

Downloaded from ajpregu.physiology.org on March 4, 2008